AGU PUBLICATIONS

Earth and Space Science

REVIEW
10.1002/2016EA000166

Key Points:
- Camera systems have been a core component of all instrument payloads sent to the Martian surface
- Context cameras on Mars have enabled 40 years of robotic field geology
- Future technical capability includes increases in spatial and spectral resolution

Correspondence to:
C. R. Cousins,
crc9@st-andrews.ac.uk

Citation:
Gunn, M. D., and C. R. Cousins (2016), Mars surface context cameras past, present, and future, *Earth and Space Science*, *3*, doi:10.1002/2016EA000166.

Received 26 FEB 2016
Accepted 27 MAR 2016
Accepted article online 7 APR 2016

Mars surface context cameras past, present, and future

M. D. Gunn[1] and C. R. Cousins[2]

[1]Institute of Maths, Physics and Computer Science, Aberystwyth University, Aberystwyth, UK, [2]Department of Earth and Environmental Sciences, Irvine Building, University of St Andrews, St. Andrews, UK

Abstract Mars has been the focus of robotic space exploration since the 1960s, in which time there have been over 40 missions, some successful, some not. Camera systems have been a core component of all instrument payloads sent to the Martian surface, harnessing some combination of monochrome, color, multispectral, and stereo imagery. Together, these data sets provide the geological context to a mission, which over the decades has included the characterization and spatial mapping of geological units and associated stratigraphy, charting active surface processes such as dust devils and water ice sublimation, and imaging the robotic manipulation of samples via scoops (Viking), drills (Mars Science Laboratory (MSL) Curiosity), and grinders (Mars Exploration Rovers). Through the decades, science context imaging has remained an integral part of increasingly advanced analytical payloads, with continual advances in spatial and spectral resolution, radiometric and geometric calibration, and image analysis techniques. Mars context camera design has encompassed major technological shifts, from single photomultiplier tube detectors to megapixel charged-couple devices, and from multichannel to Bayer filter color imaging. Here we review the technological capability and evolution of science context imaging instrumentation resulting from successful surface missions to Mars, and those currently in development for planned future missions.

1. Introduction

In 1971, the first image captured from the Martian surface was transmitted back to Earth from the Soviet Mars 3 lander (Figure 1). The image captured was only a partial one, due to the termination of lander transmissions 20 s into the mission, and without any discernible features due to exceptionally low levels of illumination courtesy of an ill-timed global dust storm [*Johnson*, 1979]. Despite this, the first image of the Martian surface represented the birth of Mars surface exploration, and since then over 150,000 full frame in situ images have been transmitted back to Earth by subsequent surface missions. From these images, sedimentary successions [*Squyres et al*., 2004; *Grotzinger et al*., 2005; *Squyres and Knoll*, 2005; *Squyres et al*., 2009; *Grotzinger et al*., 2015], hydrated and alteration minerals [*Johnson et al*., 2007; *Parente et al*., 2009; *Rice et al*., 2010; *Nachon et al*., 2014], meteorite falls [*Domokos et al*., 2007; *Schröder et al*., 2008], near-surface water ice [*Smith et al*., 2009], atmospheric properties and phenomena [*Greeley et al*., 2004, 2006; *Lemmon et al*., 2004; *Bell et al*., 2006a; *Greeley et al*., 2010; *Lemmon et al*., 2015], astronomical observations [*Pollack et al*., 1978; *Bell et al*., 2004, 2005], and volcanic processes [*Squyres et al*., 2007] have been visually identified in situ on the surface of Mars.

Robotic field geology is implicit in the surface exploration of Mars, not only to answer geological questions associated with the formation and evolution of the planet but also to provide the paleoenvironmental context to geochemical and organic analyses undertaken by other instruments within a lander payload [*Smith et al*., 1997a; *Crisp et al*., 2003; *Griffiths et al*., 2006; *Grotzinger et al*., 2012; *Vaniman et al*., 2014; *Crumpler et al*., 2015]. Instrument payloads evolve through every mission cycle, depending on the science goals of a particular surface mission. Previous payloads have included instruments to characterize the elemental geochemistry of rocks and soils, such as the Alpha Particle X-ray Spectrometer (APXS) instrument on board the two Mars Exploration Rovers (MERs) Spirit and Opportunity [*Rieder et al*., 2003] and the ChemCam Laser-Induced Breakdown Spectrometer system on Mars Science Laboratory (MSL) Curiosity [*Maurice et al*., 2012]. Likewise, instrument payloads have further evolved to detect and analyze trace organic compounds, such as Sample Analysis on Mars (SAM) gas chromatograph-mass spectrometer-tunable laser spectrometer system on MSL Curiosity [*Mahaffy et al*., 2012] and the Mars Organics Molecule Analyzer (MOMA) mass spectrometer instrument under development for the 2018 ExoMars rover [*Brinckerhoff et al*., 2015]. Over the decades, science context imaging technology has been a mainstay of all instrument payloads, for the simple reason that the identification of geological features and their spatial distribution requires

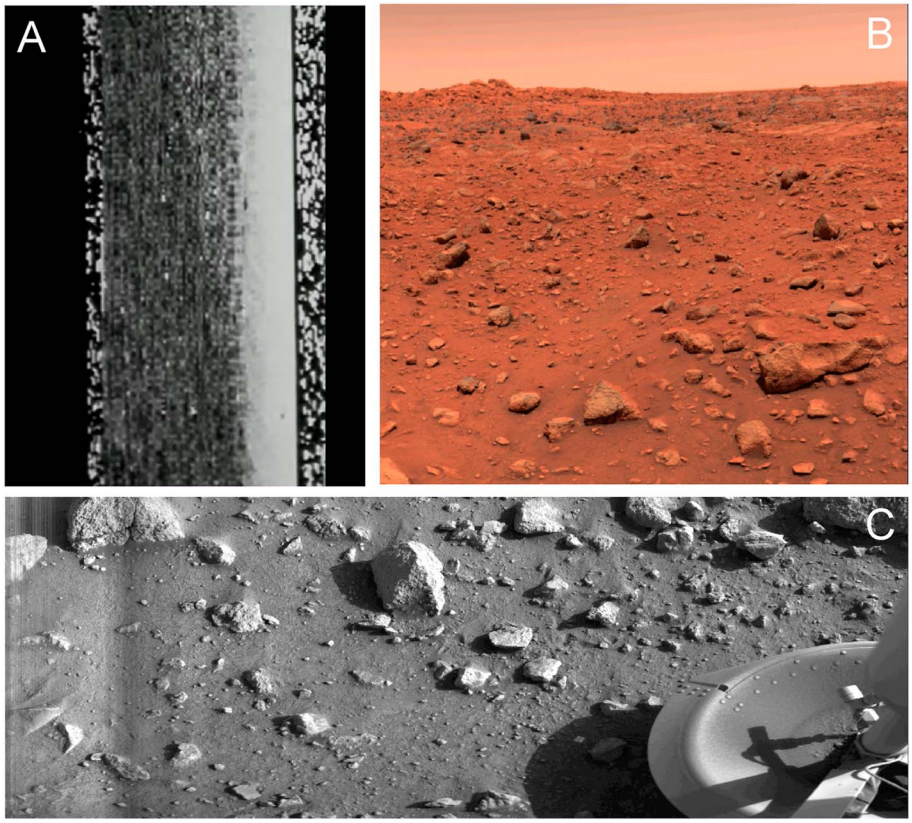

Figure 1. First images transmitted back from the Martian surface. (a) The first image transmitted from the Martian surface, from the Soviet Mars 3 lander in 1971 (courtesy of the Soviet Academy of Sciences). (b) The first color image (PIA00563) of the Martian surface from the NASA Viking Lander 1 Camera 2 in 1976 (courtesy of NASA/Jet Propulsion Laboratory-California Institute of Technology (JPL-Caltech)). (c) The first clear image (PIA00381) transmitted from the Martian surface in 1976 from the NASA Viking Lander 1 Camera 2 at Chryse Planitia (courtesy of NASA/JPL-Caltech). The lander foot can be seen bottom right.

image data that are representative of human and enhanced visual capability. From these images, local lithologies, mineralogy, geomorphology, and stratigraphic and temporal associations can be established, and targets for further investigation selected. Examples of panoramic images captured from the Martian surface across the decades are shown in Figure 2. Representative imaging of the Martian surface is vital for exploration and will continue to form an integral component of future missions, including the first sample caching and first sample return missions. As instrument payloads have advanced, imaging technology has also become incorporated into high-resolution analytical instrumentation, including the MSL ChemCam instrument [*Maurice et al*., 2012], MicrOmega instrument [*Pilorget and Bibring*, 2013] scheduled for the 2018 European Space Agency (ESA) ExoMars mission, and the SuperCam instrument recently selected for the NASA Mars2020 sample caching mission [*Gasnault et al*., 2015]. These advances demonstrate the increasing requirement for spatially resolved contextualized data, at millimeter scales, particularly in combination with mineralogical or compositional data.

Imaging technology has changed significantly over the four decades of space exploration. Some of the earliest cameras sent into space used photographic film [*Johnson*, 1979]. Image data were transmitted back to Earth for storage and reconstruction after the film was exposed, chemically developed and scanned with a serial scanner on board the spacecraft. Although these camera systems were heavy and mechanically complex, they produced high-quality images. Indeed, photographic film cameras on board the Soviet Union's Luna 3 orbiter captured the first images of the farside of the Moon in 1959. Although film cameras were flown on the Soviet Mars 1 orbiter in 1960, it became necessary to find a lighter and simpler imaging technology for planetary surface deployment. Two principal technologies have since been used in Mars lander camera systems: serial scanning cameras and framing cameras based on focal plane arrays. The main

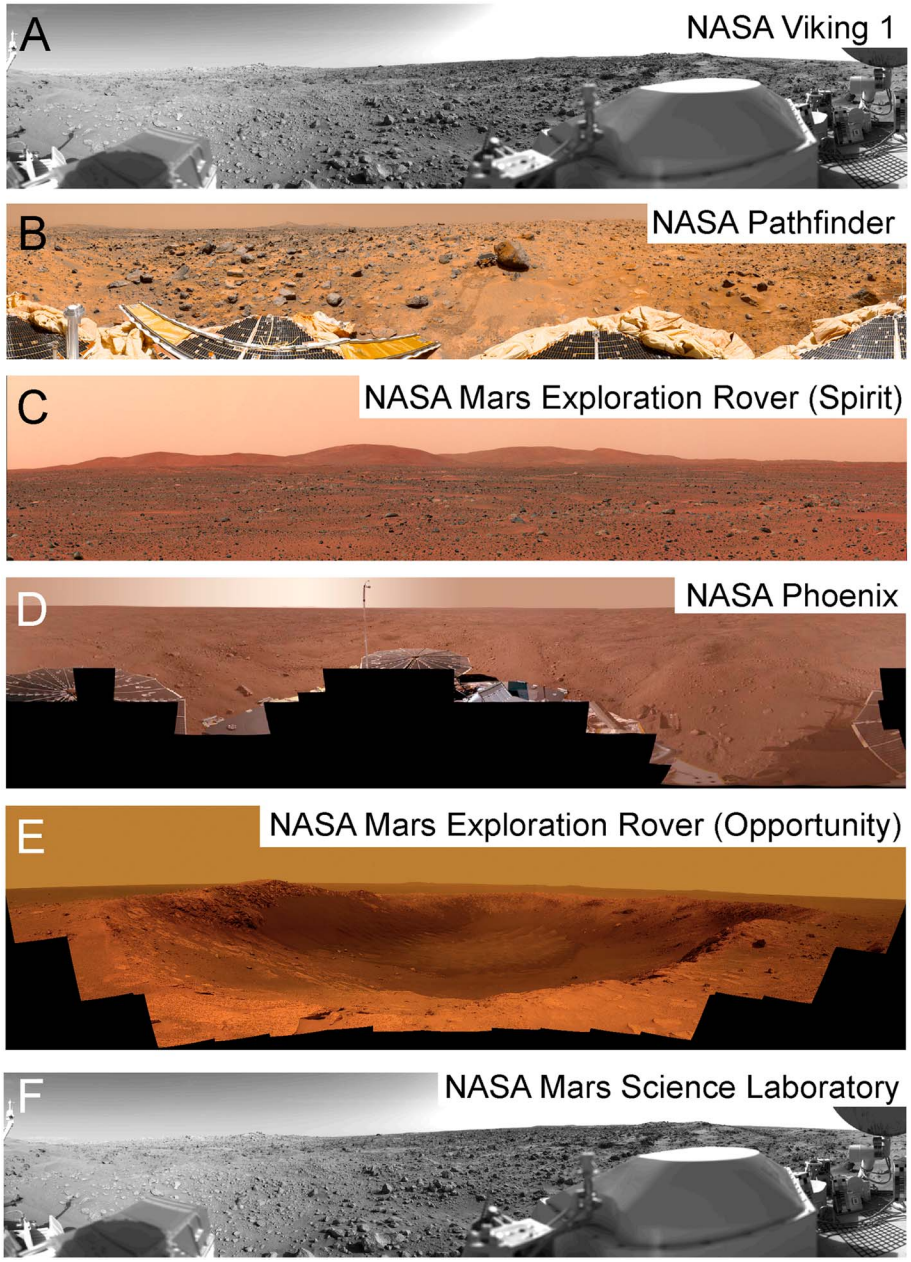

Figure 2. Martian panoramas over the decades. (a) The 1976 NASA Viking 1, Camera 2, first panorama at Chryse Planitia (PIA00383; courtesy of NASA/JPL); (b) 1997 NASA Pathfinder, IMP, Ares Vallis (PIA00994; courtesy of NASA/JPL); (c) 2004 NASA MER Spirit, Pancam, Gusev Crater (PIA05061; courtesy of NASA/JPL/Cornell); (d) 2008 NASA Phoenix, SSI, Vastitas Borealis (PIA11007; courtesy of NASA/JPL-Caltech/University of Arizona/Texas A&M University); (e) 2010 NASA MER Opportunity, Pancam, Santa Maria crater (PIA13794; courtesy of NASA/JPL-Caltech/Cornell/ASU); and (f) 2014 NASA MSL, Mastcam, "Rocknest" looking east toward Point Lake (PIA16453; courtesy of NASA/JPL-Caltech/Malin Space Science Systems).

specifications of scientific context cameras flown on successful surface missions to Mars are summarized in Table 1 and described in this paper. For this purpose we define "science context camera" here to be any imaging system that is not primarily used for navigation or hazard identification, such as the "navcams" and "hazcams" on the Mars Exploration Rovers (MERs) and MSL rover, as these have predominantly operational responsibilities. Likewise, those cameras used primarily for "close-up" or "macro" imaging, such as the Microscopic Imager (MI) on the MERs, the Mars Hand Lens Imager (MAHLI) and ChemCam on MSL, or the Close-Up Imager (CLUPI) on the ExoMars rover are also not included, as these have a dominantly analytical role for preselected targets.

Table 1. Properties of the Viking Lander Camera Photodiodes[a]

Photodiode	Photodiode Rational	Spatial Properties	Spectral Properties (λ and BW; nm)	
1	Survey scan	Angular resolution 0.12°, optimum focus at	Panchromatic	
2	Solar	3.7 M giving in focus images from 1.7 m to ∞	Panchromatic, no amplification	
			λ	BW
3	Color: blue		480	~85
4	Color: green		550	~60
5	Color: red		675	~125
6	Infrared		875	~95
7	Infrared		950	~70
8	Infrared		990	~95
9–12	4 times high resolution	Angular resolution 0.04°, optimum focus at 1.9, 2.7, 4.5, and 13.3 m	Panchromatic	

[a]CWL: center wavelength; BW: bandwidth. Geometric details from *Patterson et al.* [1977] and spectral properties from *Huck et al.* [1977].

2. Mars Surface Cameras 1971–2012

2.1. Mars 3 Cycloramic Cameras

In 1971, the Soviet Union's Mars 3 probe was the first spacecraft to successfully make a soft landing on the Martian surface [*Huntress et al.*, 2003]. Unfortunately, the lander failed after transmitting only 20 s of data (Figure 1). It has been suggested that its failure was the result of a corona discharge [*Huntress et al.*, 2003] caused by what was believed to be the largest dust storm ever observed on the planet up to the time of landing. The lander was a roughly spherical structure with four segmented "petals" which opened to self-right the lander and expose the instruments, plus a tethered rover; "Prop-M" [*Perminov*, 1999]. In addition to the two cycloramic cameras, the lander carried a mass spectrometer, atmospheric sensors (temperature, pressure, and wind), and other instruments to determine the mechanical properties of the Martian surface [*Johnson*, 1979; *Perminov*, 1999].

The two Mars 3 cameras were serial imaging cycloramic cameras of the same design as those employed on the Soviet Luna landers [*Johnson*, 1979]. The cameras were designed to capture 360° monochrome panoramic images using a photoelectron Multiplier Tube detector [*Johnson*, 1979]. The two cameras, with a small separation of approximately 120 mm, were also capable of producing stereoscopic images [*Perminov*, 1999], although none were returned from the mission. Overall, this design represented a significant advance in camera design as it was smaller and lighter than the previous film-based instruments and had the potential to capture an almost unlimited number of images.

2.2. Viking Lander Facsimile Cameras

The NASA Viking Landers 1 and 2 successfully touched down in 1976 and returned scientific data to Earth until communication was lost in 1980 and 1982 [*Huntress et al.*, 2003]. The three-legged landers each carried a 91 kg suite of scientific instruments including two facsimile camera systems ("Camera 1" and "Camera 2"), a seismometer, metrology sensors (wind direction, velocity, air temperature, and atmospheric pressure), a robotic arm with a temperature sensor, magnet and sample scoop, a biology experiment, and an X-ray fluorescence spectrometer [*Soffen and Young*, 1972; *Klein et al.*, 1976]. The landers were each powered by two Radioisotope Thermoelectric Generator (RTG) units [*Soffen and Young*, 1972] which provided electrical power by converting the decay heat of plutonium-238 into electricity using thermopiles. The long half-life of Pu-238 (87.7 years) allowed the landers to continue to operate without a significant loss of power for many years. During their long missions the two landers returned a wealth of information about the Martian surface environment and geology [*Viking Lander Team*, 1978]. This included the first close-up images of the surface in the visible (Figure 1) and infrared, and demonstration of the contextual value of surface imaging [*Binder et al.*, 1977; *Moore et al.*, 1977]. The information gathered during these missions was used to define the objectives and payloads of subsequent missions, albeit after a long hiatus in surface exploration until the NASA Pathfinder mission in 1997.

The cameras on the NASA Viking Landers operated on the same principle as the Mars 3 cameras but were larger, heavier, and more advanced. Although they were operated as serial scanning cameras, they had an array of 12 photodiode detectors (Table 1) allowing them to capture high-resolution panchromatic images

as well as lower resolution images in red, green, and blue and three infrared spectral bands [*Huck et al*., 1977]. Consequently, the Viking Lander cameras were the first multispectral cameras to be used on Mars. The assignments and properties of the 12 photodiodes are summarized in Table 2. The field of view within a single frame was fixed vertically but could be defined in azimuth and offsets could be used to allow much greater scene coverage than could be achieved with the Mars 3 cameras. The Viking 1 Lander returned the first complete image ever seen of the Martian surface (Figure 1), including color, panchromatic, and infrared images. These images were subsequently used as a benchmark for the design of (and resulting data products for) successive Mars surface cameras.

2.3. Imager for Mars Pathfinder

More than 20 years after the launch of the Viking missions, the next Martian surface probe was the NASA Mars Pathfinder mission. Pathfinder was developed as a low-cost feasibility study into the use of mobile rovers on the Martian surface [*Golombek et al*., 1999] and consisted of a static lander with a small mobile rover ("Sojourner"). The static lander not only served primarily as a communications relay for the Sojourner rover but also carried the mast-mounted stereo multispectral camera system—the Imager for Mars Pathfinder (IMP) used for surveying the landing site [*Smith et al*., 1997a]. In addition to the IMP, the lander carried the wind socks and magnetic properties experiments which were monitored by the IMP [*Smith et al*., 1997b] and a metrology instrument package [*Golombek et al*., 1999]. The Sojourner rover itself carried its own cameras (monochrome and color, not reviewed here), an Alpha Proton X-ray spectrometer, optical sensors to monitor the rate of dust accumulation, and a mechanical abrasion experiment [*Golombek et al*., 1999]. A folded optical path allowed the whole of the IMP camera to be contained within a compact cylindrical housing (Figure 3). The elevation axis was coaxial with the cylindrical housing, with the optical axis raised slightly to improve the cameras' ability to look downward [*Smith et al*., 1997a]. The camera head was mounted on a sprung glass fiber open lattice mast which was coiled up into a canister for launch. After landing, the mast was released and self-deployed to raise the camera to the working height of 1.75 m.

In the two decades between the launch of the Viking and Pathfinder missions, imaging technology had significantly advanced and the Imager for Mars Pathfinder (IMP) was the first of the Mars lander cameras to operate in framing imaging mode. Multispectral capabilities were achieved with filter wheels containing band-pass interference filters to select different spectral bands (Table 3), instead of the photodiode detector array employed for the Viking Lander cameras. The IMP made use of a 512×512 pixel charge-coupled device (CCD) detector operated in frame transfer mode so that only the top half of the array (512×256 pixels) was used to collect light. The bottom half of the array was covered with aluminum and used as the readout buffer [*Kramm et al*., 1998]. A folded optical path allowed the single CCD to capture two images from spatially separated "eyes" simultaneously through different lenses and filter wheels to give stereoscopic data. At the end of an exposure the accumulated charge was transferred rapidly to the covered lower half of the array where it was sequentially transferred to the readout electronics and digitized [*Smith et al*., 1997a]. Because each eye exposed only a quarter of the CCD, the image resolutions were relatively low at 250×256 pixels (12 pixels between the two images were shaded by a baffle). Each eye of the IMP had its own filter wheel to allow independent selection of spectral bands (Table 3), with a total of 24 filter slots available. The filters in the wheel were to be used for different science objectives, and with the 443, 671, and 998 nm filters duplicated in both eyes so that stereo data sets could be generated. A total of 12 narrowband "geology" filters covering the Visible and Near Infra-Red (VNIR) spectral region were included to distinguish between Fe^{3+} and Fe^{2+} mineral types, along with seven filters for solar observations and a panchromatic channel with a diopter lens for close-up imaging [*Smith et al*., 1997a].

By the end of the Pathfinder mission, the IMP returned over 16,500 images [*Kramm et al*., 1998; *Golombek et al*., 1999] and contributed significantly to the knowledge of the Martian environment. In addition to characterizing the rocks and soils at the landing site (Figure 4h), IMP images were also used to observe the wind socks [*Smith et al*., 1997a] for measuring wind speed and direction, and to monitor evidence of aeolian processes [*Smith et al*., 1997b]. Images of the Sun and sky at different times of the day and night were used to determine the opacity of the atmosphere, characterize atmospheric aerosols, and determine water vapor abundance [*Smith et al*., 1997b]. Nighttime images were taken of the Martian moons to provide spectroscopic information and measure their albedo [*Smith et al*., 1997b]. Overall, the IMP instrument had successfully demonstrated the utility of stereoscopic, multispectral camera systems in the exploration of Mars. The Surface Stereo Imager (SSI) that was part of the Mars Volatiles and Climate Surveyor (MVACS) payload on

Table 2. Summary of Technical Specifications for the Mars Science Context Cameras On Board Past Successful, Currently Ongoing, and Upcoming Missions[a]

	Past Missions				Current Missions		Upcoming Missions
Name	Soviet Mars 3 Lander Cycloramic Cameras [*Johnson*, 1979; *Perminov*, 1999]	NASA Viking Lander Camera 1 and Camera 2 [*Mutch et al.*, 1972; *Huck et al.*, 1976; *Patterson et al.*, 1977; *Viking Lander Team*, 1978]	NASA Mars Pathfinder Imager for Mars Pathfinder (IMP) [*Smith et al.*, 1997a]	NASA Phoenix Surface Stereo Imager (SSI) [*Lemmon et al.*, 2008; *Smith et al.*, 2008; *Moores et al.*, 2010; M. Lemmon, personal communication, 2015]	NASA MER Panoramic Camera (Pancam) [*G. H. Smith et al.*, 2001; *Bell et al.*, 2003; *Smith*, 2006]	NASA MSL Mastcam (M34 (L) and M100 (R)) [*Ghaemi*, 2009; *Bell et al.*, 2012; *Malin et al.*, 2010; *DiBiase et al.*, 2012; *Maki et al.*, 2012]	ESA/Roscosmos ExoMars Panoramic Camera (Pancam) [*Griffiths et al.*, 2006; *Harris et al.*, 2015]
Configuration	Two serial imaging mode "cycloramic telephotometer" cameras, vertical scanning	Two serial mode "Facsimile" cameras, vertical scanning	Single frame transfer monochrome CCD camera split between two eyes with separate filter wheels	Two-frame transfer CCD camera split between two eyes with separate filter wheels	Two-frame transfer CCD camera split between two eyes with separate filter wheels	Two color Bayer filter CCDs with filter wheels and optics with internal variable focus	Two multispectral wide-angle cameras (WACs) with filter wheels and one high-resolution camera (HRC) using RGB filter stripes
Camera elevation (m)	1 (estimated)	0.556	1.75	0.84 above deck	1.54	2	1.7
Sensor (s)	FEU-54 photomultiplier tube	12 photodiodes	512 × 512 CCD	1024 × 1024 CCD	1024 × 2048 Mitel (DALSA) frame transfer CCDs	Kodak KAI-2020 interline transfer CCD with Bayer array color filter	Star 1000 radiation hard CMOS Active Pixel Sensor (APS)
Pixel size $H \times V$ (μm)	NA	NA	23 × 23 including 6 μm antiblooming channel	12 × 12	12 × 12	7.4	15 × 15 [*Uwaerts*, 2006]
Stereo separation (mm)	Approximately 120	800	150	150	300	200	500
Toe in	NA	NA	L: 0.72°, R: 1.4°, overlap at 4 m	1.37°, overlap at 3 m	1°, overlap at 10 m	Unknown	2.8°
Angular resolution/pixel	0.06° (estimated)	Low resolution: 0.12° High resolution: 0.04°	0.057°	0.014°	0.016°	M34: 0.012°, M100: 0.0042°	WACs: 0.033°; HRC: 0.005°
Field of view ($H \times V$; deg)	360° × 29°	Low resolution: 2.5–352.5° × 61.44° High resolution: 2.5–352.5° × 20.48°	14.4° × 14°	13.8° × 13.8°	16° × 16°	M34: 18.4° × 15°; M100: 6.3° × 5.1°	WACs: 34° × 34°; HRC: 5° × 5°
Exposure times and mode	NA	NA	0 to 32 s in 0.5 ms increments; autoexposure available	0 to 335 s in 5.12 ms increments	0 to 335 s in 5.12 ms increments; autoexposure and relative exposure times for geology filters	Auto or commanded	Unknown
Frame rate	4 lines/s 25 min/full panoramic frame	Time per degree in azimuth Rapid scan: survey 1.84 s, color and	2 s readout after frame transfer for full array, 1 s for left eye only	5.2 s readout after frame transfer	5.2 s readout after frame transfer	10/s at 720 pixels HD 5/s at full resolution (http://www.jpl.	Unknown

AGU Earth and Space Science 10.1002/2016EA000166

AGU Earth and Space Science 10.1002/2016EA000166

Table 2. (continued)

	Past Missions				Current Missions		Upcoming Missions
Name	Soviet Mars 3 Lander Cycloramic Cameras [*Johnson*, 1979; *Perminov*, 1999]	NASA Viking Lander Camera 1 and Camera 2 [*Mutch et al.*, 1972; *Huck et al.*, 1976; *Patterson et al.*, 1977; *Viking Lander Team*, 1978]	NASA Mars Pathfinder Imager for Mars Pathfinder (IMP) [*Smith et al.*, 1997a]	NASA Phoenix Surface Stereo Imager (SSI) [*Lemmon et al.*, 2008; *Smith et al.*, 2008; *Moores et al.*, 2010; M. Lemmon, personal communication, 2015]	NASA MER Panoramic Camera (Pancam) [*G. H. Smith et al.*, 2001; *Bell et al.*, 2003; *Smith*, 2006]	NASA MSL Mastcam (M34 (L) and M100 (R)) [*Ghaemi*, 2009; *Bell et al.*, 2012; *Malin et al.*, 2010; *DiBiase et al.*, 2012; *Maki et al.*, 2012]	ESA/Roscosmos ExoMars Panoramic Camera (Pancam) [*Griffiths et al.*, 2006; *Harris et al.*, 2015]
		high-resolution 5.52 s (250 bits/s) Slow scan: survey 2 min, color and high resolution 6 min (16,000 bits/s)				nasa.gov/missions/)	
Scene coverage ($H \times V$; deg)	360° × 29°	342.5° × 100° (40° above to 60° below the horizon)	360° × 157° (zenith to 67° below horizon)	360° × 150° (zenith to 60° below horizon)	360° × 180°	360° × 178° (91° up to 87° down)	360° × 180°
Image resolution	6000 × 500	512 samples per line	Two 248 × 256 images on CCD.6	1024 × 1024	1024 × 1024	1600 × 1200	1024 × 1024
Spectral capability	Panchromatic	12 photodiodes each: four high resolution at different focus; six low-resolution color and IR; low-resolution panchromatic and low-resolution solar (no amplification)	12 slots per wheel; 15 geology and 8 solar filters, 1 dioptre	12 filters per wheel for geological and atmospheric studies	8 filters per wheel; 16 total	12 filters per wheel	WACs: 11 filters per wheel, HRC: 3 filter stripes (R, G, B)
Dynamic range/SNR	Unknown	6 bit, SNR survey: 420 color and high resolution: ~220	12 bit, SNR 350	SNR >200 at 50% full well	SNR >200 at 50% full well	Unknown	Unknown
Lens type	Unknown	Achromatic triplet	Cooke triplet	Cooke triplet	Cooke triplet	M34: eight elements (five static and three focus); M100: nine elements (six static and three focus)	Four-element air spaced
Lens focal length	Unknown	57.3 mm	23 mm	49.98 mm	43 mm	M34: 34 mm; M100: 100 mm	21.85 mm
Lens *F*#	Unknown	*f*/5.6	*f*/18	*f*/20.2	*f*/20	M34: *f*/8; M100: *f*/10	*f*/10
Focus	Fixed at a hyperfocal distance of 3 m, in focus 1.5 m to ∞	High resolution: four photodiodes with sharp focus at 1.9, 2.7, 4.5, and 13.3 m	Sharp focus at 1.3 m	Cameras: best focus at 3 m, good focus 2 m to ∞	Best focus at 3 m	Variable focus 2 m to ∞	WACs: fixed focus, DOF 1 m to ∞

Table 2. (continued)

	Past Missions				Current Missions		Upcoming Missions
Name	Soviet Mars 3 Lander Cycloramic Cameras [*Johnson*, 1979; *Perminov*, 1999]	NASA Viking Lander Camera 1 and Camera 2 [*Mutch et al.*, 1972; *Huck et al.*, 1976; *Patterson et al.*, 1977; *Viking Lander Team*, 1978]	NASA Mars Pathfinder Imager for Mars Pathfinder (IMP) [*Smith et al.*, 1997a]	NASA Phoenix Surface Stereo Imager (SSI) [*Lemmon et al.*, 2008; *Smith et al.*, 2008; *Moores et al.*, 2010; M. Lemmon, personal communication, 2015]	NASA MER Panoramic Camera (Pancam) [*G. H. Smith et al.*, 2001; *Bell et al.*, 2003; *Smith*, 2006]	NASA MSL Mastcam (M34 (L) and M100 (R)) [*Ghaemi*, 2009; *Bell et al.*, 2012; *Malin et al.*, 2010; *DiBiase et al.*, 2012; *Maki et al.*, 2012]	ESA/Roscosmos ExoMars Panoramic Camera (Pancam) [*Griffiths et al.*, 2006; *Harris et al.*, 2015]
		Low resolution: hyperfocal distance of 3.7 m, in focus 1.7 m to ∞	Depth of field 0.5 m to ∞	Deck filters: best focus 1 to 1.4 m	Depth of field 1.5 m to ∞		HRC: variable, 0.98 m to ∞
Camera mass	1.3 kg each	7.26 kg each including electronics	5.2 kg including pan-tilt unit (http://www.jpl.nasa.gov/missions/)	Camera head and mast 4.46 kg, electronics 0.91 kg	267 g per camera including electronics box	<0.9 kg per camera	WACs 200 g each; HRC 300 g; total 1.75 kg including optical bench and electronics
Power consumption	2.5 W	Low resolution: 34 W High resolution: 27 W	2.6 W (http://www.jpl.nasa.gov/missions/)	4.2 W idle; 11.8 W imaging; 51.2 W peak	Per camera: 1.4 W (idle); 2.4 W (integration and readout); 3.8 W (fast flush)	Unknown	WACs: 1.5 W; HRC: 0.9 W
Additional hardware	NA	Geometric and radiometric calibration targets; magnets; wind vane; dust blower	Radiometric standard reflectors; magnetic properties investigation; three wind socks	"iSweep" calibration targets with magnets; "Telltail" mechanical anemometer	Sundial calibration target; 3.5 W strip heaters attached to electronics boxes; filter wheels	Calibration target, fiducial markers	Pancam Calibration Target (PCT) and Rover Inspection Mirror (RIM)
Images returned	1 partial (79 lines). See Figure 1a	Viking 1 and 2 combined, nearly 6600	16500 [*Golombek et al.*, 1999]	29930	MER A Spirit: 29,501. MER B Opportunity: 40,654 and increasing (full frame) (http://merweb.sese.asu.edu/mer_edr_counter.pl)	88,609 Experimental Data Record (EDR) images and increasing (Planetary Data System (PDS))	NA

[a]Unless otherwise stated, data are from the reference(s) at the top of the column. NA: not available.

AGU Earth and Space Science

10.1002/2016EA000166

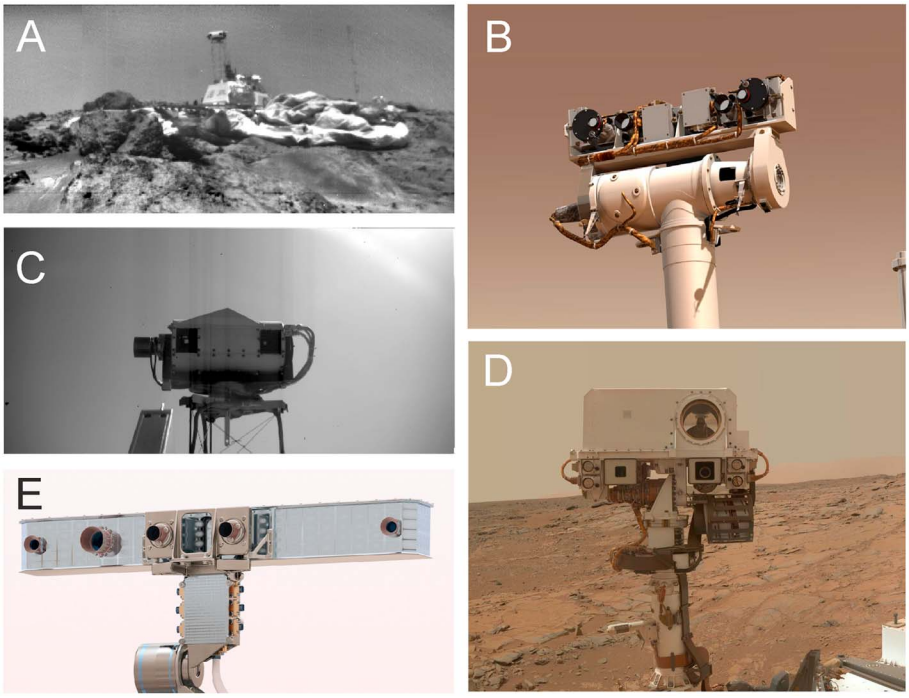

Figure 3. Mars context cameras past and present. (a) The IMP fully deployed on the NASA Pathfinder lander, imaged from the Sojourner rover camera (PIA01121, courtesy of NASA/JPL). (b) Artist concept of the NASA Mars Exploration Rover, cropped to show Pancam positioned at the top of the mast (courtesy of NASA/JPL/Cornell University). (c) Self-portrait of the SSI on the NASA Phoenix lander, imaged by the Robotic Arm Camera at the Martian surface (PIA11223, courtesy of NASA/JPL-Caltech/University of Arizona/Max Planck Institute). (d) Cropped self-portrait of the Mastcam (two lower cameras below ChemCam) on the MSL rover Curiosity imaged by the MAHLI instrument, at the Martian surface (PIA16937, courtesy of NASA/JPL-Caltech/MSSS). (e) Cropped artist concept of the PanCam instrument on board the planned ESA/Roscosmos 2018 ExoMars rover, showing the position of the two WACs (either end) and HRC (off-center camera) within the ExoMars optical bench (courtesy of ESA).

the ill-fated 1999 NASA Mars Polar Lander (MPL) mission was an almost exact copy of the IMP. The only significant difference between the instruments was the data bus interfacing them with the rest of the lander [*P. H. Smith et al.*, 2001]. Communication with MPL was not reestablished following the landing sequence, and the craft was declared lost. The mission failure has been attributed to a software glitch which caused the decent engines to shut down while the craft was at an altitude of approximately 40 m [*Euler et al.*, 2001].

2.4. Mars Exploration Rover Panoramic Camera

Following the successful demonstration of the benefits of a mobile rover to Mars exploration, larger rovers were developed with comprehensive scientific instrument packages to investigate the Martian geology [*Crisp et al.*, 2003]. The Mars Exploration Rovers Spirit and Opportunity were the first truly mobile Martian surface missions and were capable of traversing the Martian terrain at a top speed of 4 cm/s on flat surfaces [*Crisp et al.*, 2003]. The two identical rovers each carried a suit of robotic arm-mounted instruments including a Mossbauer spectrometer, Rock Abrasion Tool, Microscopic Imager, and Alpha Particle X-ray Spectrometer. The stereo multispectral panoramic camera (Pancam) [*Bell et al.*, 2003] was mounted on the mast, as were the collecting optics for the Miniature Thermal Emission Spectrometer (Mini-TES) [*Crisp et al.*, 2003]. The body of the rovers carried a suit of engineering sensors including hazard avoidance and navigation cameras, as well as the solar panels, magnetic sweep experiment, and the Pancam calibration target [*Crisp et al.*, 2003]. The objective for both rovers was to cover at least 600 m over their 90 Martian solar days (sols) primary missions [*Crisp et al.*, 2003], and both remain amongst the most successful Mars surface missions to date, lasting significantly longer than the planned mission duration.

The MER panoramic cameras (Pancams) consist of 1024×2048 frame transfer CCDs with an active area of 1024×1024 pixels. The CCDs are coupled with Cooke triplet objectives and 11-position filter wheels (Table 3) all mounted in a dust-sealed enclosure with a sapphire window [*G. H. Smith et al.*, 2001; *Bell et al.*, 2003].

Table 3. Filter Properties and Their Respective Purposes for Mars Context Science Cameras That Utilize a CCD Detector Framing Camera Interfaced With a Filter Wheel [*Smith et al.*, 1997a, 1997b; *Bell et al.*, 2003; *Lemmon et al.*, 2008; *Bell et al.*, 2012; *Cousins et al.*, 2012]

	NASA Mars Pathfinder IMP			NASA MER A and B Pancam			NASA Phoenix SSI			NASA MSL Mastcam			ESA/Roscosmos ExoMars PanCam[a]		
	Primary Purpose[b]	λ	BW	Primary Purpose[b]	λ	BW	Primary Purpose[b]	λ	BW	Primary Purpose[b]	λ	BW	Primary Purpose[b]	λ	BW
							Left Camera								
L1	Geology	443	26	Pan	739	338	Stereo, Geology	673	19	Vis	590	172	Geology	481	28
L2	Solar	450	4.9	Stereo	753	20	Stereo, Geology	447	23	Geology	527	14	Geology	439	22
L3	Solar	883	5.6	Geology	673	16	Solar	451	4.1	Geology	445	20	Geology	532	32
L4	Solar	925	5	Geology	601	17	Solar	991	4.9	Geology	751	20	Geology	751	18
L5	Solar	935	4.8	Geology	535	20	Solar	887	5.8	Geology	676	10	Geology	857	34
L6	Geology	671	20	Geology	482	30	Geology	833	28	Geology	867	20	Geology	930	32
L7	Geology	802	21	Geology, Stereo	432	32	Geology	802	22	Geology	1012	42	Geology, Stereo	669	17
L8	Geology	858	34	Solar	440	20	Geology	864	37	Solar	880	20	DiopF, Stereo	671	17
L9	Geology	898	41	-	-	-	Geology	900	45	-	-	-	Solar	928	5.5
L10	Geology	931	27	-	-	-	Geology	931	25	Bayer, Color	495	74	Solar	936	5.6
L11	Geology	1003	29	-	-	-	Geology	1002	26	Bayer, Color	554	76	Solar	1000	6
L12	Geology	968	31	-	-	-	Geology	968	30	Bayer, Color	640	88	Solar	877	6
							Right Camera								
R1	Geology	443	26	Stereo	436	37	Stereo, Geology	673	19	Vis	575	180	Pan	720	560
R2	Solar	670	5.3	Stereo	754	20	Stereo, Geology	447	23	Geology	527	14	Geology	602	21
R3	Solar	946	44	Geology	803	20	Solar	671	4.9	Geology	447	20	Geology	799	20
R4	Solar	936	4.9	Geology	864	17	Solar	936	5.2	Geology	805	20	Geology	906	42
R5	Solar	989	5.4	Geology	904	26	Solar	936	5.2	Geology	908	22	Geology	961	29
R6	Geology	671	20	Geology	934	25	DiopN	450	29	Geology	937	22	Geology	1003	28
R7	Geology	752	19	Geology	1009	38	DiopN	753	20	Geology	1013	42	DiopF	668	17
R8	DiopN, Pan			Solar	880	20	Geology	754	21	Solar	440	20	DiopF, Color, Stereo	668	18
R9	Geology	600	21	-	-	-	LP	753	17	-	-	-	DiopF, Color	440	22
R10	Geology	531	30	-	-	-	Geology	604	15	Bayer, Color	493	76	DiopF, Color	532	32
R11	Geology	480	27	-	-	-	Geology	532	28	Bayer, Color	551	78	Solar	449	4
R12	Geology	967	30	-	-	-	Geology	485	21	Bayer, Color	638	88	Solar	670	5.5

[a]Filter positions are unfinalized.
[b]Filter purpose: Geology—filters to select for different mineralogical and compositional absorption bands; Bayer—Bayer filter channels on MSL Mastcam cameras; Color—for color image generation; DiopF—diopter for far focus (for focussing on distant objects with the baseline ExoMars Pancam); DiopN—diopter for near focus (for focusing on the deck of the Phoenix lander and the tip plate magnet (190 mm distance) on Pathfinder); LP—linear polarizer; Pan—panchromatic (no filter); Stereo—stereo image capture for digital elevation model (DEM) generation; Solar—solar filter (typically has an optical density of 4 or 5 (OD5 = 10^{-5} transmittance) for direct imaging of the Sun); Vis—visible spectral region filter (IR cut).

The cameras are mounted on the camera bar on top of the mast which also carries the two navigation cameras [*Bell et al.*, 2003; *Crisp et al.*, 2003] as shown in Figure 3. All the science and engineering cameras on board the MERs use identical sensors and electronics [*Maki et al.*, 2003] which were so successful that they were also used for the Phoenix Surface Stereo Imager [*Lemmon et al.*, 2008] and the MSL rover "Curiosity" engineering cameras [*Maki et al.*, 2012]. The pan-tilt unit also points the aperture of the Mini-TES instrument [*Christensen et al.*, 2003], which itself is housed in the warm electronics box in the body of the rover [*Crisp et al.*, 2003]. This enables the Mini-TES to be scanned as a whiskbroom hyperspectral imager to produce low-resolution thermal emission images coincident with the Pancam images. The Pancam cameras themselves are mechanically very simple and have proved to be extremely reliable. As with most of the previous Martian lander cameras, the MER Pancams used small aperture, fixed focus Cooke triplet lenses [*G. H. Smith et al.*, 2001; *Smith*, 2006]. This lens configuration is well suited to planetary lander applications as they are optically and mechanically simple, can be corrected over relatively wide fields of view, and can achieve diffraction-limited performance at the small apertures generally employed. All glass elements in the lens assemblies must be air spaced, as cemented elements with different thermal expansion coefficients would be likely to separate after repeated thermal cycling on the Martian surface [*Smith*, 2006].

Between them, the Pancams on the two rovers have returned over 70,587 full frame images and counting (http://merweb.sese.asu.edu/mer_edr_counter.pl) from the Martian surface and contributed significantly to the knowledge of the Martian environment and geology. In particular, the large volume of data generated allowed extensive work on the identification and classification of rock and soil lithologies to be carried out using the multispectral images, developing new multispectral image processing techniques to enhance

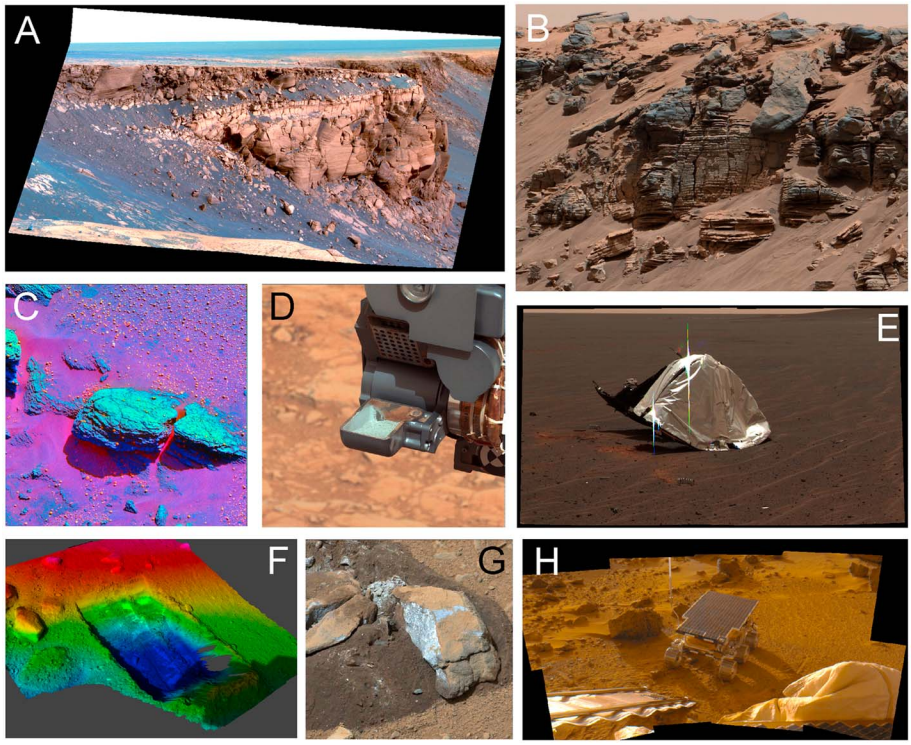

Figure 4. Examples of science outputs from Mars science context cameras. (a) False color image of aeolian sediment with cross-bedding exposed on the Cape St. Vincent promontory along Victoria Crater (PIA09695; courtesy of NASA/JPL/Cornell), imaged by the MER Pancam on board Opportunity. (b) True color image of laminated lacustrine sediments near "Hidden Valley" (PIA19074; courtesy of NASA/JPL-Caltech/MSSS), imaged by the MSL Mastcam on the Curiosity rover (central outcrop ~50 cm across). (c) False color multispectral image of a sedimentary outcrop with spherules, enhancing the compositional phases present (PIA05236; courtesy of NASA/JPL/Cornell), imaged by the MER Pancam on the Opportunity rover. (d) MSL Curiosity's first powdered drill sample within the rover's scoop (4.5 cm wide) prior to sieving and analysis, as imaged by Mastcam and white balanced to terrestrial illumination (PIA16729, courtesy of NASA/JPL-Caltech/MSSS). (e) MER Opportunity two-frame true color mosaic generated from Pancam using 480, 530, and 600 nm filters, showing heat shield debris (1.3 m high) from the MER mission (PIA07224; courtesy of NASA/JPL/Cornell). (f) Color shaded elevation map of the 22 cm wide "Dodo-Goldilocks" trench dug by the robotic arm on board the Phoenix lander (PIA10904; courtesy of NASA/JPL-Caltech/University of Arizona/Texas A&M University/NASA Ames Research Center). (g) Loose surface rock broken by the Curiosity rover wheel to reveal a fresh internal surface (PIA16804, courtesy of NASA/JPL-Caltech/MSSS/ASU). (h) Eight-image mosaic acquired by the Pathfinder IMP (530, 600, 750 nm filters) showing the newly deployed Sojourner rover (PIA01551; courtesy of NASA/JPL).

and exploit subtle spectral differences within the local terrain to aid geological interpretation (Figure 4a). Techniques such as band stretching, Spectral Mixture Analysis (SMA), and classification methods including Principal Component Analysis (PCA) and spectral parameters [*Farrand et al*., 2006, 2007, 2008; *Rice et al*., 2010; *Farrand et al*., 2013] have been used to analyze surface data with great effect (Figure 4).

2.5. Phoenix Lander Surface Stereo Imager

The Phoenix lander was the first probe to return surface data from the north polar region of Mars following the loss of the Mars Polar Lander in 1999. As with the Mars Polar Lander, Phoenix was designed to explore buried water reservoirs within the northern polar region of Mars and to characterize the presence and interaction of volatile phases within surface soils [*Smith et al*., 2008]. A priority for the mission was to dig through the surface soil to search for (and analyze) water ice detected below the Martian surface by the Mars Odyssey Orbiter in 2002 [*Smith et al*., 2008]. The landers scientific payload included a multispectral panoramic stereo camera (the Surface Stereo Imager, SSI), optical and atomic force microscopes, an electrochemistry and conductivity analyzer, thermal and evolved gas analyzer, a suit of metrological instruments, a magnetic dust properties experiment, and a robotic arm for digging and sample collection which was also equipped with a camera [*Smith et al*., 2008].

The SSI on the Phoenix lander was based closely on the IMP [*Smith et al*., 1997a] and the SSI on Mars Polar Lander [*P. H. Smith et al*., 2001]. However, rather than the single CCD shared between both eyes as with the IMP and Mars Polar Lander SSI, the Phoenix SSI used two 1024 pixel square CCDs, the same sensors (flight spares) as the MER Pancams [*Moores et al*., 2010]. These were mounted in a very similar camera head to that used for IMP (Figure 3). The only significant modifications to the IMP camera head design were to make space for the two CCDs in place of the single one on IMP. As with the IMP and Mars Polar Lander SSI, the Phoenix SSI was mounted on an open lattice sprung mast which could be deployed once the lander was safely on the surface. Image data from the Phoenix SSI were heavily utilized to provide the scientific and structural context to the soil-sampling component of the mission, which was achieved with a scoop on the end of the robotic arm [*Smith et al*., 2008]. Color, monochrome, and stereo data revealed polygonal ground typical of permafrost terrains [*Mellon et al*., 2009; *Smith et al*., 2009], water ice and perchlorates [*Smith et al*., 2009; *Cull et al*., 2010], and the three-dimensional morphology and depth of the trenches dug and samples by the robotic arm (Figure 4f).

2.6. Mars Science Laboratory Mastcam

The Mars Science Laboratory (MSL) rover Curiosity is the most technically advanced Mars rover to date and is by far the largest lander to be sent to the Martian surface. Powered by an RTG, the rover is designed to cover large distances on the Martian surface during its primary mission of one Martian year [*Grotzinger et al*., 2012]. The MSL surface mission has now been ongoing for over 1196 sols during which time it has covered more than 13.6 km (http://curiosityrover.com/tracking/drivelog.html). One of its main mission objectives is to search for evidence of "habitability," including the identification of any organic compounds and building up an inventory of the chemical building blocks of life found at the Martian surface [*Grotzinger et al*., 2012]. It will also continue to characterize the Martian surface geology and measure the Martian radiation environment [*Grotzinger et al*., 2012]. Curiosity carries an array of instruments including a high-resolution stereo color and multispectral camera system, a long standoff Laser-Induced Breakdown Spectroscopy (LIBS) and camera instrument (ChemCam) with a useful range of up to 7 m, the Sample Analysis at Mars (SAM) instrument suite, X-ray diffraction and fluorescence instruments, radiation detectors, an environmental monitoring station, and a robotic arm equipped with an Alpha Particle X-ray Spectrometer, hand lens imager camera, drill, sample collection scoop, and a brush to remove dust from rock surfaces [*Grotzinger et al*., 2012].

The mast-mounted camera ("Mastcam") system on the Curiosity rover is a departure from the configuration used for previous Mars surface cameras. Rather than two identical monochrome cameras with multispectral capability via a set of filter wheels, Mastcam employs two Bayer filter array color cameras with different focal lengths. The Mastcam lenses have focal lengths of 34 and 100 mm [*Ghaemi*, 2009] and incorporate the variable focus mechanisms developed for the MAHLI camera [*Ghaemi*, 2009; *Malin et al*., 2010]. The 34 mm Mastcam has a similar field of view to the previous NASA lander cameras of around 15°, while the 100 mm Mastcam provides much higher spatial resolution over a field of view of approximately 5°. This difference in field of view means it is more difficult to obtain data products that rely on images from both left and right cameras, such as stereo data products, and multispectral image sets (as the filters are distributed between the cameras). However, this overall configuration has the advantage that both wide-angle context images and close-up detailed images can be captured without moving the rover (Figure 4). The detectors in Mastcam have a 4×3 format with 1600×1200 pixels (~2 megapixels). Rather than using monochrome CCDs with filters to produce color images with three exposures, Mastcam uses a Bayer color filter array to obtain color images in a single exposure [*Malin et al*., 2010], enabling high-resolution color images to be regularly acquired. The trade-off with this approach is that when the narrowband geology filters (Table 3) in the visible region of the spectrum are used, the images are captured using only one of the Bayer color channels, effectively quartering the resolution of the detector. However, this is mitigated by a large detector size. All three of the Bayer filter channels transmit more or less equally above 850 nm, and so in the infrared the full resolution of the CCDs is achieved [*Bell et al*., 2012]. The high pixel density and fast readout and storage electronics mean that Mastcam cameras can also capture 720 pixels HD video at eight frames per second [*Malin et al*., 2010]. None of the previous Mars lander cameras could achieve even a single frame per second, and as such this represents an entirely new aspect of surface imaging. The new lenses incorporating adjustable focus with fixed focal length are far more complex than those on previous Mars camera systems. With eight and nine optical elements, respectively [*Ghaemi*, 2009], the M34 and M100 lenses have at least doubled the number of optical surfaces of even the most complex lens on MER cameras, such as the four-element Hologon/Biogon design of the wide-angle Navcam lenses [*G. H. Smith et al*., 2001; *Smith*, 2006].

3. Future Mars Surface Cameras

3.1. NASA InSight

The imaging capability on the NASA InSight lander, planned for launch in 2018, will represent a departure from the traditional "robotic field geology" approach employed by previous missions, particularly exploration rovers. Specifically, InSight is the first surface mission focused primarily on establishing the geophysical properties of the Martian interior with an instrument suite including a seismometer, a heat flow probe, and an X-band transponder [*Banerdt et al*., 2013]. The cameras on board InSight therefore will be primarily to perform an engineering purpose, aiding the successful deployment of the core instrument payload, rather than investigate the local geological context of the surface environment in scientific detail. For this, InSight will have two cameras; a 45 × 45° field of view (FOV) Instrument Deployment Camera, which will be used to create 3-D digital elevation models from stereo pairs for detailed terrain assessment (e.g., as done for the Phoenix lander), and a 124° FOV Instrument Context Camera [*Trebi-Ollennu et al*., 2013].

3.2. ExoMars 2018

ExoMars is a two-part European Space Agency mission aimed at establishing if life has ever existed on Mars. The first part of the mission will consist of an orbiter containing instruments including a trace gas analyzer to search for methane in the Martian atmosphere. An entry, descent and landing technology demonstrator will be carried to Mars with the orbiter, which was successfully launched in 2016. The second part of the ExoMars mission will be a solar-powered rover currently under development by ESA in collaboration with Roscosmos. The rover planned for launch in 2018 or 2020 will carry the Pasteur science payload, which currently consists of a mast-mounted panoramic camera (Pancam), a Close-Up Imager (CLUPI), ground-penetrating radar, the Infrared Spectrometer for ExoMars (ISEM), and a drill combined with a spectrometer to reach up to 2 m into the Martian surface to take spectra and collect samples. Collected drill samples will be analyzed by internal analytical instruments including an infrared hyperspectral microscope (MicrOmega [*Pilorget and Bibring*, 2013]), Raman spectrometer [*Rull et al*., 2011], and Organic Molecule Analyzer (MOMA [*Brinckerhoff et al*., 2015]).

The ExoMars PanCam is a suite of three cameras mounted in an optical bench (Figure 3) on top of the ExoMars rover mast. ExoMars PanCam consists of a pair of wide-angle cameras (WACs) with multispectral capabilities and a stereo separation of 500 mm, and a high-resolution camera (HRC) with color imaging capabilities mounted off center as shown in Figure 3. The wide-angle camera design is based on the earlier Stereo Camera System on board the failed Beagle2 lander [*Griffiths et al*., 2005], and the panoramic cameras on the canceled Netlander mission [*Jaumann et al*., 2003]. The instrument is still under development, and so any specifications given are based on the current design iteration [see *Coates et al*., 2012 and *Harris et al*., 2015]. The WACs have a wide 38.6° field of view, and hence relatively low angular resolution. This is countered by the inclusion of the HRC, which will allow distant features of interest to be imaged remotely in color and at high spatial resolution. Like the Pathfinder IMP and MER Pancams, the ExoMars PanCam produces multispectral data products via a filter wheel interfaced to each WAC, in this case each with 11 filter positions. Of these 22 filters, 12 are dedicated to geology, with center wavelengths and band passes optimized to be sensitive to subtle spectral variations of Mars-relevant minerals in the 400–1000 nm spectral range detectable by PanCam [*Cousins et al*., 2010, 2012]. The remaining filters are dedicated to broadband color (six filters, two each for red, green, and blue) and four solar filters [*Coates et al*., 2012].

Since the ExoMars PanCam instrument is still under development, it is not yet possible to compare its performance with previous camera systems. However, a PanCam emulator has been deployed in Mars analogue terrains [*Harris et al*., 2015]. This demonstrated the multispectral utility of the ExoMars PanCam in the detection of past habitability, and the value of HRC images for target selection [*Harris et al*., 2015].

3.3. Mars2020

The Mars2020 rover will carry the Mastcam-Z camera system [*Bell et al*., 2014]. Mastcam-Z derives heritage from the MSL Mastcam instrument, utilizing almost exact copies of the electronics and sensors. However, unlike the MSL Mastcam, Mastcam-Z incorporates two matching 3.6:1 zoom lenses to cover horizontal fields of view from 23° to 6°. This will allow the instrument to produce stereo and multispectral data sets with matching fields of view from both cameras. The zoom mechanism is based on that originally developed and qualified for Mastcam, but with the zoom range descoped from the original 15:1 [*Bell et al*., 2014]. As

for MSL Mastcam, Mastcam-Z is likely to carry a pair of solar filters, a set of geology filters, and a broadband visible filter for color imaging using the Bayer array. As such, Mastcam-Z will represent a new phase of technical configuration for science camera systems deployed on Mars.

4. Calibration and Science Outputs

Vital to context science cameras on all past, current, and future missions is the correct calibration and processing of image data sent back from the Martian surface. As with camera hardware technology, downstream image processing has advanced dramatically in order to enhance scientific outputs [*Alexander et al*., 2006], especially to aid the geological interpretation of the outcrops (Figures 4a–4c) and enhance subtle surface features [e.g., *Greenberger et al*., 2015]. Image products include (i) the generation of anaglyphs from stereo pairs for 3-D visualization, (ii) color calibration and white balancing to view surface geology in both Mars true color and simulated terrestrial illumination, and (iii) enhancement of mulitspectral channels to highlight subtle compositional and structural features otherwise missed in color or monochrome images (Figure 4). Much of this image processing was developed during the MER mission, which saw Pancam heavily utilized to great effect for target selection and geological context. This included the regular exploitation of multispectral image data [*Bell et al*., 2004; *Farrand et al*., 2006, 2007, 2008; *Rice et al*., 2010; *Weitz et al*., 2010; *Farrand et al*., 2013], detailed analysis of the spectrophotometric properties of various rocks and soils [*Johnson et al*., 2006b, 2006c], and the development of spectral unmixing techniques to identify mineralogical end-member components within Pancam data sets [*Parente et al*., 2009]. Conversely, white-balancing of MSL Mastcam data to terrestrial illumination conditions has been a more widely used approach and has proven especially useful for revealing the contrast between the heavily oxidized red-colored surface and the more reduced, grey-colored nature of subsurface sedimentary deposits sampled by the drill [*Kah and the MSL Science Team*, 2015]. Multispectral processing has been utilized most effectively in mapping the spatial distribution of hydrated mineral features, particularly diagenetic calcium sulfate veins [*Vaniman et al*., 2014]. Finally, building up of repeated image sequences has enabled temporal observations to be made of mineralogical [*Rice et al*., 2011], atmospheric [*Greeley et al*., 2010; *Moores et al*., 2010], and water ice sublimation [*Smith et al*., 2009] features.

Such image processing is entirely reliant on correct in situ calibration. For this, all missions from Viking onward have incorporated a dedicated calibration target to be included within image sequences. In situ measurements of a calibration target with accurately known reflectance properties allows otherwise purely radiometric measurements to be processed to obtain relative reflectance [*Bell et al*., 2006b]. Radiometric calibration targets consist of a number of gray scale and colored calibration patches mounted on the lander in clear view of the camera system, and in locations where they will be as free as possible from shadows and light scattered from other parts of the lander structure. Calibration patches are calibrated for both absolute total hemispherical reflectance and Bidirectional Reflectance Distribution Function (BRDF) to allow the relative positions of the Sun and camera to be accounted for [*Wall et al*., 1975; *Bell et al*., 2003, 2006b; *Smith et al*., 1997a]. The design of calibration targets varies, but most have included a shadow post as shown in Figure 5. This allows direct measurement of the position and angle of the Sun and enables the contribution of indirect illumination scattered by the atmosphere to be assessed.

The calibration patches of all NASA landers from Pathfinder onward have been composed of Room Temperature Vulcanized (RTV) Silicone rubber colored with mineral pigments [*Smith et al*., 1997a; *Bell et al*., 2003; *Leer et al*., 2008]. This material is a bulk scatterer providing an even scattering distribution. However, the material surface properties have meant it has a high affinity for dust adhesion [*Sabri et al*., 2012] and so the prevalent Martian dust reduces the effectiveness of the calibration targets as the mission progresses [*P. H. Smith et al*., 2001; *Bell et al*., 2006b; *Johnson et al*., 2006a; *Kinch et al*., 2007]. Periodic Martian storms have been observed to reduce the dust cover on both the calibration targets and the solar panels, but a layer of dust is always preserved. As such, optical models have been developed to account for the effects of dust on the reflectance properties of the calibration targets and allow them to continue to be used [*Bell et al*., 2006b; *Johnson et al*., 2006a; *Kinch et al*., 2007]. To reduce this phenomenon, the ExoMars PanCam Calibration Target (PCT) calibration patches will be composed of stained glass [*Barnes et al*., 2011], selected for its high resistance to solarization (UV-induced discoloration). It had also been observed that the glass patch on the Curiosity Mars Hand Lens Imager (MAHLI) calibration patch has a lower affinity for the adhesion

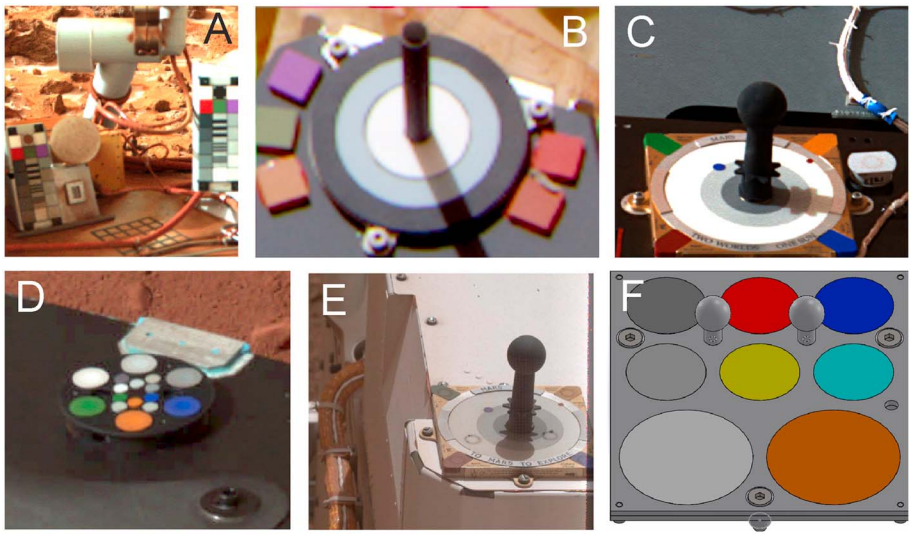

Figure 5. Calibration targets used for calibrating context camera data on (a) Viking (PIA00573; courtesy of NASA/JPL), (b) Pathfinder (PIA00620; courtesy of NASA/JPL/University of Arizona), (c) MER (PIA05018; courtesy of NASA/JPL/Cornell University), (d) Phoenix (PIA10720; courtesy of NASA/JPL-Caltech/University of Arizona/Texas A&M University), and (e) MSL Curiosity (Sol3, L0 filter; courtesy of NASA/MSSL). (f) Current design for the 2018 ExoMars rover (courtesy of M. Gunn, Aberystwyth University).

of Marian dust compared to the silicon patches on its calibration target. Finally, magnets have been included in previous calibration targets both to allow analysis of the magnetic fraction of the airborne dust and to screen regions of the calibration target from dust settling [*Leer et al*., 2008; *Drube et al*., 2010]. However, it was found that the magnets had the opposite effect and increased the dust coverage of the "protected" regions in comparison to calibration target patches without magnets [*Drube et al*., 2010].

5. Evolution of Camera Design

Over a period of more than four decades a number of landers have been sent to investigate the surface of Mars, and new landers are currently under development for launch in the future. Each of the past landers has carried a camera system with which to image the Martian surface, enable the selection of science targets, and provide scientific context to the results of other instruments. All recent cameras (IMP onward) have been framing mode multispectral imagers with CCD detectors and filter wheels. Although there have been refinements in specification as new camera systems are developed, the basic design and capabilities of the cameras has changed little since the IMP. The relatively recent inclusion of high-resolution camera capability as part of the science context camera system for MSL Curiosity (high-resolution lens in Mastcam) and ExoMars (HRC in PanCam) allows features of interest observed with the wide-angle cameras to be examined in greater detail without the need to maneuver the rover into close proximity. This allows a much greater number of potential targets to be examined in detail during the mission and as such increases the science output. Likewise, the image sensors of the cameras on for MSL Curiosity and Mars2020 are 2 megapixels [*Ghaemi*, 2009] and so have double the resolution of than those on previous cameras. Although not a context camera, the Close-Up Imager (CLUPI) on the ExoMars rover utilizes a 14 megapixel Foveon sensor which has three stacked arrays of 2652 × 1768 pixels to capture color images instead of the more conventional Bayer filter array [*Josset et al*., 2014]. If these continue to be successful, these developments could pave the way for cameras with much higher resolutions than those flown previously, representing the next evolutionary stage in science context imaging.

As well as increases in spatial resolution, there are developments toward the increase of spectral resolution of context camera systems with multispectral filter wheel technologies inherited from IMP being superseded by hyperspectral imagers using technologies such as whiskbroom spectrometers (ISEM [*Ivanov et al*., 2014] and ChemCam [*Maurice et al*., 2012]), pushbroom imaging spectrographs (Ultra Compact Imaging Spectrometer [*Van Gorp et al*., 2014]), and windowing [*Sellar and Boreman*, 2005] linear variable interference filters

(HyperCLUPI [*Barnes et al*., 2014]). While filter wheels have proved reliable, the limitation to a restricted number of predetermined wavelengths does not allow for serendipitous or unexpected discoveries to be easily mitigated for. Likewise, the inclusion of a Bayer filter on both MSL Mastcam and Mars2020 Mastcam-Z signify a reduction in the reliance on filter wheels, at least for the production of color composite images. Given the inherent spectral limitation of using a silicon CCD ($<1\,\mu m$) for multispectral studies, future multispectral capability within context cameras may move altogether toward infrared imagers, building on existing instruments such as the Mini-TES on the MER rovers [*Christensen et al*., 2003], and focusing on tunable filter systems, such as Acousto-Optic Tunable Filters. However, the developments in spatial and spectral resolution of camera technologies are not currently matched by increases in data bandwidth of the communication systems, and so it is unlikely that these technologies will find regular and widespread use in the immediate future. In spite of this many of these instruments could be used a much lower resolution the majority of the time, with their full capabilities only being used when the need arises.

6. Conclusions

Science context cameras have played an essential role in robotic field geology on Mars since surface exploration began four decades ago. In this time, their technology has evolved well beyond basic color representation to incorporate increasing spectral and spatial capability and downstream image manipulation. While remote robotic surface visualization is no substitute for human "eyes on the ground" exploration, it provides an unprecedented window into extraterrestrial geology that has yet to be matched for any other planetary surface beyond Earth. In this sense, Mars has played a vital role in providing an effective training ground for science camera technology.

Acknowledgments
Matthew Gunn and Claire Cousins are Coinvestigators on the European Space Agency ExoMars panoramic camera instrument (PI Andrew Coates; MSSL/University College London, London, United Kingdom). C. Cousins is funded by the Royal Society of Edinburgh on a Personal Research Fellowship. Matthew Gunn acknowledges UK Space Agency grants ST/L001454/1, ST/N003349/1, and ST/N006410/1. All data used are listed in the references and tables. Finally, we thank two anonymous reviewers for their timely and helpful comments on the manuscript.

References

Alexander, D. A., R. G. Deen, P. M. Andres, P. Zamani, H. B. Mortensen, A. C. Chen, M. K. Cayanan, J. R. Hall, V. S. Klochko, O. Pariser, and C. L. Stanley (2006), Processing of Mars Exploration Rover imagery for science and operations planning, *J. Geophys. Res.*, *111*, E02S02, doi:10.1029/2005JE002462.

Banerdt, W. B., S. Smrekar, P. Lognonné, T. Spohn, S. W. Asmar, D. Banfield, L. Boschi, U. Christensen, V. Dehant, W. Folkner, and D. Giardini (2013), InSight: A discovery mission to explore the interior of Mars, 44th Lunar Planet. Sci. Conf., held March 18–22, 2013 in the Woodlands, Texas, LPI Contrib. 1719, p.1915.

Barnes, D., M. Wilding, M. Gunn, L. Tyler, S. Pugh, A. Coates, A. Griffiths, C. Cousins, N. Schmitz, and G. Paar (2011), The PanCam Calibration Target (PCT) and multispectral image processing for the ExoMars 2018 mission, EPSC-DPS Joint Meeting 2011, vol. 1, p. 289. 2011.

Barnes, D., et al. (2014), Developing a Hyperspectral Close-Up Imager with UV excitation (HyperCLUPI) for Mars exploration, European Planetary Science Congress 2014, EPSC Abstracts, Vol. 9, EPSC2014-729.

Bell, J. F. III, et al. (2003), Mars Exploration Rover Athena panoramic camera (Pancam) investigation, *J. Geophys. Res.*, *108*(E12), 8063, doi:10.1029/2003JE002070.

Bell, J. F., et al. (2004), Pancam multispectral imaging results from the Opportunity Rover at Meridiani Planum, *Science*, *306*(5702), 1703–1709, doi:10.1126/science.1105245.

Bell, J. F., M. T. Lemmon, T. C. Duxbury, M. Y. H. Hubbard, M. J. Wolff, S. W. Squyres, L. Craig, and J. M. Ludwinski (2005), Solar eclipses of Phobos and Deimos observed from the surface of Mars, *Nature*, *436*(7047), 55–57, doi:10.1038/nature03437.

Bell, J. F., D. Savransky, and M. J. Wolff (2006a), Chromaticity of the Martian sky as observed by the Mars Exploration Rover Pancam instruments, *J. Geophys. Res.*, *111*, E12S05, doi:10.1029/2006JE002687.

Bell, J. F. III, J. Joseph, J. N. Sohl-Dickstein, H. M. Arneson, M. J. Johnson, M. T. Lemmon, and D. Savransky (2006b), In-flight calibration and performance of the Mars Exploration Rover panoramic camera (Pancam) instruments, *J. Geophys. Res.*, *111*, E02S03, doi:10.1029/2005JE002444.

Bell, J. F., M. C. Malin, M. A. Caplinger, M. A. Ravine, A. S. Godber, M. C. Jungers, M. S. Rice and R. B. Anderson (2012), Mastcam multispectral imaging on the Mars Science Laboratory rover: Wavelength coverage and imaging strategies at the Gale Crater field site, 43rd Lunar Planet. Sci. Conf., held March 19–23, 2012 at The Woodlands, Texas, LPI Contrib. 1659, id.2541.

Bell, J. F., J. N. Maki, G. L. Mehall, M. A. Ravine and M. A. Caplinger (2014), Mastcam-Z: A geologic, stereoscopic, and multispectral investigation on the NASA Mars-2020 Rover, International Workshop on Instrumentation for Planetary Missions, Greenbelt, Maryland.

Binder, A. B., R. E. Arvidson, E. A. Guinness, K. L. Jones, E. C. Morris, T. A. Mutch, D. C. Pieri, and C. Sagan (1977), The geology of the Viking Lander 1 site, *J. Geophys. Res.*, *82*(28), 4439–4451, doi:10.1029/JS082i028p04439.

Brinckerhoff, W., et al. (2015), Mars Organic Molecule Analyzer (MOMA) Mass Spectrometer Status and science operations on the ExoMars Rover, 46th Lunar Planet. Sci. Conf., held March 16–20, 2015 in The Woodlands, Texas, LPI Contribution No. 1832, p.2579.

Christensen, P. R., et al. (2003), Miniature Thermal Emission Spectrometer for the Mars Exploration Rovers, *J. Geophys. Res.*, *108*(E12), 8064, doi:10.1029/2003JE002117.

Coates, A. J., et al. (2012), Lunar PanCam: Adapting ExoMars PanCam for the ESA Lunar Lander, *Planet. Space Sci.*, *74*, 247–253, doi:10.1016/j.pss.2012.07.017.

Cousins, C. R., A. D. Griffiths, I. A. Crawford, B. J. Prosser, M. C. Storrie-Lombardi, L. E. Davis, M. Gunn, A. J. Coates, A. P. Jones, and J. M. Ward (2010), Astrobiological considerations for the selection of the geological filters on the ExoMars PanCam instrument, *Astrobiology*, *10*, 933–951, doi:10.1089/ast.2010.0517.

Cousins, C. R., M. Gunn, B. J. Prosser, D. P. Barnes, I. A. Crawford, A. D. Griffiths, L. E. Davis, and A. J. Coates (2012), Selecting the geology filter wavelengths for the ExoMars panoramic camera instrument, *Planet. Space Sci.*, *71*, 80–100, doi:10.1016/j.pss.2012.07.009.

Crisp, J. A., M. Adler, J. R. Matijevic, S. W. Squyres, R. E. Arvidson, and D. M. Kass (2003), Mars Exploration Rover mission, *J. Geophys. Res.*, *108*(E12), 8061, doi:10.1029/2002JE002038.

Crumpler, L. S., et al. (2015), Context of ancient aqueous environments on Mars from in situ geologic mapping at Endeavour Crater, *J. Geophys. Res. Planets*, *120*, 538–569, doi:10.1002/2014JE004699.
Cull, S. C., R. E. Arvidson, J. G. Catalano, D. W. Ming, R. V. Morris, M. T. Mellon, and M. Lemmon (2010), Concentrated perchlorate at the Mars Phoenix landing site: Evidence for thin film liquid water on Mars, *Geophys. Res. Lett.*, *37*, L22203, doi:10.1029/2010GL045269.
DiBiase, D., J. Bardis, and R. Billing (2012), A zoom lens for the MSL mast cameras: Mechanical design and development, Proceedings of the 41st Aerospace Mechanisms Symposium, Jet Propul. Lab., May 16–18, 2012.
Domokos, A., J. F. Bell III, P. Brown, M. T. Lemmon, R. Suggs, J. Vaubaillon, and W. Cooke (2007), Measurement of the meteoroid flux at Mars, *Icarus*, *191*, 141–150, doi:10.1016/j.icarus.2007.04.017.
Drube, L., et al. (2010), Magnetic and optical properties of airborne dust and settling rates of dust at the Phoenix landing site, *J. Geophys. Res.*, *115*, E00E23, doi:10.1029/2009JE003419.
Euler, E. A., S. D. Jolly, and H. H. Curtis (2001), The failures of the Mars Climate Orbiter and Mars Polar Lander: A perspective from the people involved, *Adv. Astronaut. Sci.*, *107*, 635–655.
Farrand, W. H., J. F. Bell III, J. R. Johnson, S. W. Squyres, J. Soderblom, and D. W. Ming (2006), Spectral variability among rocks in visible and near-infrared multispectral Pancam data collected at Gusev crater: Examinations using spectral mixture analysis and related techniques, *J. Geophys. Res.*, *111*, E02S15, doi:10.1029/2005JE002495.
Farrand, W. H., et al. (2007), Visible and near-infrared multispectral analysis of rocks at Meridiani Planum, Mars, by the Mars Exploration Rover Opportunity, *J. Geophys. Res.*, *112*, E06S02, doi:10.1029/2006JE002773.
Farrand, W. H., J. F. Bell III, J. R. Johnson, R. E. Arvidson, L. S. Crumpler, J. A. Hurowitz, and C. Schröder (2008), Rock spectral classes observed by the Spirit Rover's Pancam on the Gusev Crater Plains and in the Columbia Hills, *J. Geophys. Res.*, *113*, E12S38, doi:10.1029/2008JE003237.
Farrand, W. H., J. F. Bell III, J. R. Johnson, M. S. Rice, and J. A. Hurowitz (2013), VNIR multispectral observations of rocks at Cape York, Endeavour crater, Mars by the Opportunity rover's Pancam, *Icarus*, *225*, 709–725, doi:10.1016/j.icarus.2013.04.014.
Gasnault, O., S. Maurice, R. C. Wiens, S. Le Mouélic, W. W. Fischer, P. Caïs, K. McCabe, J.-M. Reess, and C. Virmontois (2015), SuperCam remote micro-imager on Mars 2020, 46th Lunar Planet. Sci. Conf., held March 16–20, 2015 in The Woodlands, Texas. LPI Contrib. 1832, p.2990.
Ghaemi, F. T. (2009), Design and fabrication of lenses for the color science cameras aboard the Mars Science Laboratory rover, *Opt. Eng.*, *48*(10), 103002-103002-15, doi:10.1117/1.3251343.
Golombek, M. P., et al. (1999), Overview of the Mars Pathfinder mission: Launch through landing, surface operations, data sets, and science results, *J. Geophys. Res.*, *104*(E4), 8523–8553, doi:10.1029/98JE02554.
Greeley, R., et al. (2004), Wind-related processes detected by the Spirit rover at Gusev Crater, Mars, *Science*, *305*, 810–813.
Greeley, R., et al. (2006), Gusev crater: Wind-related features and processes observed by the Mars Exploration Rover Spirit, *J. Geophys. Res.*, *111*, E02S09, doi:10.1029/2005JE002491.
Greeley, R., D. A. Waller, N. A. Cabrol, G. A. Landis, M. T. Lemmon, L. D. V. Neakrase, M. Pendleton Hoffer, S. D. Thompson, and P. L. Whelley (2010), Gusev Crater, Mars: Observations of three dust devil seasons, *J. Geophys. Res.*, *115*, E00F02, doi:10.1029/2010JE003608.
Greenberger, R. N., J. F. Mustard, B. L. Ehlmann, D. L. Blaney, E. A. Cloutis, J. H. Wilson, R. O. Green, and A. A. Frawman (2015), Imaging spectroscopy of geological samples and outcrops: Novel insights from microns to meters, *GSA Today*, *25*(12), 4–10, doi:10.1130/GSATG252A.1.
Griffiths, A. D., A. J. Coates, J. L. Josset, G. Paar, B. Hofmann, D. Pullan, P. Ruffer, M. R. Sims, and C. T. Pillinger (2005), The Beagle 2 stereo camera system, *Planet. Space Sci.*, *53*, 1466–1482, doi:10.1016/j.pss.2005.07.007.
Griffiths, A. D., A. J. Coates, R. Jaumann, H. Michaelis, G. Paar, D. Barnes, J. -L. Josset, and the PanCam Team (2006), Context for the ESA ExoMars rover: The panoramic camera (Pancam) instrument, *Int. J. Astrobiol.*, *5*, 269–275, doi:10.1017/S1473550406003387.
Grotzinger, J. P., et al. (2005), Stratigraphy and sedimentology of a dry to wet eolian depositional system, Burns formation, Meridiani Planum, Mars, *Earth Planet. Sci. Lett.*, *240*, 11–72, doi:10.1016/j.epsl.2005.09.039.
Grotzinger, J. P., et al. (2012), Mars Science Laboratory mission and science investigation, *Space Sci. Rev.*, *170*, 5–56, doi:10.1007/s11214-012-9892-2.
Grotzinger, J. P., et al. (2015), Deposition, exhumation, and paleoclimate of an ancient lake deposit, Gale crater, Mars, *Science*, *350*, 6257, aac7575, doi:10.1126/science.aac7575.
Harris, J. K., C. R. Cousins, M. Gunn, P. M. Grindrod, D. Barnes, I. A. Crawford, R. E. Cross, and A. J. Coates (2015), Remote detection of past habitability at Mars-analogue hydrothermal alteration terrains using an ExoMars panoramic camera Emulator, *Icarus*, *252*, 284–300, doi:10.1016/j.icarus.2015.02.004.
Huck, F. O., E. E. Burcher, D. J. Jobson, and S. D. Wall (1976), Prediction of Viking Lander Camera Image Quality, in NASA Technical Notes.
Huck, F. O., D. J. Jobson, S. K. Park, S. D. Wall, R. E. Arvidson, W. R. Patterson, and W. D. Benton (1977), Spectrophotometric and color estimates of the Viking Lander sites, *J. Geophys. Res.*, *82*(28), 4401–4411, doi:10.1029/JS082i028p04401.
Huntress, W. T., V. I. Moroz, and I. L. Shevalev (2003), Lunar and Planetary Robotic Exploration missions in the 20th century, *Space Sci. Rev.*, *107*, 541–649, doi:10.1023/A:1026172301375.
Ivanov, A., O. Korablev, S. Mantsevich, N. Vyazovetskiy, A. Fedorova, N. Evdokimova, A. Stepanov et al. (2014) AOTF near-IR spectrometers for study of Lunar and Martian surface composition, European Planetary Science Congress 2014, EPSC Abstracts, Vol. 9, id. EPSC2014-371, vol. 9, p. 371. 2014.
Jaumann, R., H. G. Grothues, Y. Langevin, P. Eng, and V. Formisano (2003), The panchromatic stereo panorama camera system onboard the Netlander surface modules, EGS-AGU-EUG Joint Assembly, Abstracts from the meeting held in Nice, France, 6–11 April 2003, abstract #6009.
Johnson, J. R., et al. (2006a), Radiative transfer modeling of dust-coated Pancam calibration target materials: Laboratory visible/near-infrared spectrogoniometry, *J. Geophys. Res.*, *111*, E12S07, doi:10.1029/2005JE002658.
Johnson, J. R., et al. (2006b), Spectrophotometric properties of materials observed by Pancam on the Mars Exploration Rovers: 1. Spirit, *J. Geophys. Res.*, *111*, E02S14, doi:10.1029/2005JE002494..
Johnson, J. R., et al. (2006c), Spectrophotometric properties of materials observed by Pancam on the Mars Exploration Rovers: 2. Opportunity, *J. Geophys. Res.*, *111*, E12S16, doi:10.1029/2006JE002762.
Johnson, J. R., J. F. Bell III, E. Cloutis, M. Staid, W. H. Farrand, T. McCoy, M. Rice, A. Wang, and A. Yen (2007), Mineralogic constraints on sulfur-rich soils from Pancam spectra at Gusev crater, Mars, *Geophys. Res. Lett.*, *34*, L13202, doi:10.1029/2007GL029894.
Johnson, N. L. (1979), *Handbook of Soviet Lunar and Planetary Exploration—Volume 47 Science and Technology Series*, Am. Astronaut. Soc., Springfield, VA.
Josset, J. L., A. Souchon, M. Josset, and C. Cockell (2014), ExoMars CLUPI instrument testing at MINAR II. In European Planetary Science Congress 2014, EPSC Abstracts, Vol. 9, id. EPSC2014-658, vol. 9, p. 658. 2014.

Kah, L. C., and the MSL Science Team (2015), Images from Curiosity: A new look at Mars, *Elements*, *11*(1), 27–32, doi:10.2113/gselements.11.1.27.
Kinch, K. M., J. Sohl-Dickstein, J. F. Bell III, J. R. Johnson, W. Goetz, and G. A. Landis (2007), Dust deposition on the Mars Exploration Rover panoramic camera (Pancam) calibration targets, *J. Geophys. Res.*, *112*, E06S03, doi:10.1029/2006JE002807.
Klein, H. P., J. Lederberg, A. Rich, N. H. Horowitz, V. I. Oyama and G. V. Levin (1976) The Viking mission search for life on Mars, *Nature 262*, 5563, 24–27.
Kramm, J. R., N. Thomas, H. U. Keller, and P. H. Smith (1998), The CCD imager electronics for the Mars pathfinder and Mars surveyor cameras, *IEEE Trans. Instrum. Meas.*, *47*(5), 1112–1118, doi:10.1109/19.746566.
Leer, K., et al. (2008), Magnetic properties experiments and the Surface Stereo Imager calibration target onboard the Mars Phoenix 2007 Lander: Design, calibration, and science goals, *J. Geophys. Res.*, *113*, E00A16, doi:10.1029/2007JE003014.
Lemmon, M. T., et al. (2004), Atmospheric imaging results from the Mars exploration rovers: Spirit and Opportunity, *Science*, *306*(5702), 1753–1756, doi:10.1126/science.1104474.
Lemmon, M. T., et al. (2008), The Phoenix Surface Stereo Imager (SSI) investigation. 39th Lunar and Planetary Science Conference, (Lunar and Planetary Science XXXIX), held March 10–14, 2008 in League City, Texas. LPI Contribution No. 1391, p. 2156.
Lemmon, M. T., M. J. Wolff, J. F. Bell III, M. D. Smith, B. A. Cantor, and P. H. Smith (2015), Dust aerosol, clouds, and the atmospheric optical depth record over 5 Mars years of the Mars Exploration Rover mission, *Icarus*, *251*, 96–111, doi:10.1016/j.icarus.2014.03.029.
Mahaffy, P. R., et al. (2012), The sample analysis at Mars investigation and instrument suite, *Space Sci. Rev.*, *170*(1–4), 401–478, doi:10.1007/s11214-012-9879-z.
Maki, J., D. Thiessen, A. Pourangi, P. Kobzeff, T. Litwin, L. Scherr, S. Elliott, A. Dingizian, and M. Maimone (2012), The Mars Science Laboratory engineering cameras, *Space Sci. Rev.*, *170*(1–4), 77–93, doi:10.1007/s11214-012-9882-4.
Maki, J. N., et al. (2003), Mars Exploration Rover engineering cameras, *J. Geophys. Res.*, *108*(E12), 8071, doi:10.1029/2003JE002077.
Malin, M. C., et al. (2010), The Mars Science Laboratory (MSL) mast-mounted cameras (Mastcams) flight instruments, 41st Lunar Planet. Sci. Conf., held March 1–5, 2010 in The Woodlands, Texas. LPI Contrib. 1533, p.1123.
Maurice, S., et al. (2012), The ChemCam instrument suite on the Mars Science Laboratory (MSL) rover: Science objectives and mast unit description, *Space Sci. Rev.*, *170*, 95–166, doi:10.1007/s11214-012-9912-2.
Mellon, M. T., M. C. Malin, R. E. Arvidson, M. L. Searls, H. G. Sizemore, T. L. Heet, M. T. Lemmon, H. U. Keller, and J. Marshall (2009), The periglacial landscape at the Phoenix landing site, *J. Geophys. Res.*, *114*, E00E06, doi:10.1029/2009JE003418.
Moore, H. J., R. E. Hutton, R. F. Scott, C. R. Spitzer, and R. W. Shorthill (1977), Surface materials of the Viking landing sites, *J. Geophys. Res.*, *82*(28), 4497–4523, doi:10.1029/JS082i028p04497.
Moores, J. E., M. T. Lemmon, P. H. Smith, L. Komguem, and J. A. Whiteway (2010), Atmospheric dynamics at the Phoenix landing site as seen by the Surface Stereo Imager, *J. Geophys. Res.*, *115*, E00E08, doi:10.1029/2009JE003409.
Mutch, T. A., A. B. Binder, F. R. Huck, E. C. Levinthal, E. C. Morris, C. Sagan, and A. T. Young (1972), Imaging experiment: The Viking Lander, *Icarus*, *16*, 92–110, doi:10.1016/0019-1035(72)90139-X.
Nachon, M., et al. (2014), Calcium sulfate veins characterized by ChemCam/Curiosity at Gale crater, Mars, *J. Geophys. Res. Planets*, *119*, 1991–2016, doi:10.1002/2013JE004588.
Parente, M., J. L. Bishop, and J. F. Bell III (2009), Spectral unmixing for mineral identification in Pancam images of soils in Gusev crater, Mars, *Icarus*, *203*, 421–436, doi:10.1016/j.icarus.2009.04.029.
Patterson, W. R., F. O. Huck, S. D. Wall, and M. R. Wolf (1977), Calibration and performance of the Viking Lander cameras, *J. Geophys. Res.*, *82*(28), 4391–4400, doi:10.1029/JS082i028p04391.
Perminov, V. G. (1999), The difficult road to Mars: A brief history of Mars Exploration in the Soviet Union. Washington, D.C.: National Aeronautics and Space Administration Headquarters, Monographs in aerospace history; no. 15 01/1999; 1.
Pilorget, C., and J.-P. Bibring (2013), NIR reflectance hyperspectral microscopy for planetary science: Application to the MicrOmega instrument, *Planet. Space Sci.*, *76*, 42–52, doi:10.1016/j.pss.2012.11.004.
Pollack, J. B., J. Veverka, K. Pang, D. Colburn, A. L. Lane, and J. M. Ajello (1978), Multicolor observations of Phobos with the Viking Lander cameras: Evidence for a carbonaceous chondritic composition, *Science*, *199*(4324), 66–69, doi:10.1126/science.199.4324.66.
Rice, M. S., J. F. Bell, E. A. Cloutis, A. Wang, S. W. Ruff, M. A. Craig, D. T. Bailey, J. R. Johnson, P. A. de Souza, and W. H. Farrand (2010), Silica-rich deposits and hydrated minerals at Gusev Crater, Mars: Vis-NIR spectral characterization and regional mapping, *Icarus*, *205*, 375–395, doi:10.1016/j.icarus.2009.03.035.
Rice, M. S., J. F. Bell III, E. A. Cloutis, J. J. Wray, K. E. Herkenhoff, R. Sullivan, J. R. Johnson, and R. B. Anderson (2011), Temporal observations of bright soil exposures at Gusev crater, Mars, *J. Geophys. Res.*, *116*, E00F14, doi:10.1029/2010JE003683.
Rieder, R., R. Gellert, J. Brückner, G. Klingelhöfer, G. Dreibus, A. Yen, and S. W. Squyres (2003), The new Athena alpha particle X-ray spectrometer for the Mars Exploration Rovers, *J. Geophys. Res.*, *108*(E12), 8066, doi:10.1029/2003JE002150.
Rull, F., A. Sansano, E. Díaz, C. P. Canora, A. G. Moral, C. Tato, and C. González (2011), ExoMars Raman laser spectrometer for Exomars, in *SPIE Optical Engineering+ Applications 81520J-81520J*, International Society for Optics and Photonics, doi:10.1117/12.896787.
Sabri, F., J. G. Marchetta, M. Sinden-Redding, J. J. Habenicht, T. P. Chung, C. N. Melton, C. J. Hatch, and R. L. Lirette (2012), Effect of surface plasma treatments on the adhesion of Mars JSC 1 Simulant Dust to RTV 655, RTV 615, and Sylgard 184, *PLoS One*, *7*(11), doi:10.1371/journal.pone.0045719.
Schröder, C., et al. (2008), Meteorites on Mars observed with the Mars Exploration Rovers, *J. Geophys. Res.*, *113*, E06S22, doi:10.1029/2007JE002990.
Sellar, R., and G. Boreman (2005), Classification of imaging spectrometers for remote sensing applications, *Opt. Eng.*, *44*(1) 013602, doi:10.1117/1.1813441.
Smith, G. H. (2006), *Camera Lenses From Box Camera to Digital*, SPIE Press, Bellingham, WA.
Smith, G. H., E. C. Hagerott, L. M. Scherr, K. E. Herkenhoff, and J. F. Bell (2001), Optical designs for the Mars '03 rover cameras, in *Current Developments in Lens Design and Optical Engineering*, *Spie-Int. Soc.*, pp. 118–131, Optical Engineering. Bellingham, doi:10.1117/12.449558.
Smith, P. H., et al. (1997a), The imager for Mars Pathfinder experiment, *J. Geophys. Res.*, *102*(E2), 4003–4025, doi:10.1029/96JE03568.
Smith, P. H., et al. (1997b), Results from the Mars Pathfinder camera, *Science*, *278*, 1758–1765, doi:10.1126/science.278.5344.1758.
Smith, P. H., et al. (2001), The MVACS Surface Stereo Imager on Mars Polar Lander, *J. Geophys. Res.*, *106*(E8), 17,589–17,607, doi:10.1029/1999JE001116.
Smith, P. H., et al. (2008), Introduction to special section on the Phoenix Mission: Landing site characterization experiments, mission overviews, and expected science, *J. Geophys. Res.*, *113*, E00A18, doi:10.1029/2008JE003083.
Smith, P. H., et al. (2009), H_2O at the Phoenix landing site, *Science*, *325*, 58–61, doi:10.1126/science.1172339.
Soffen, G. A., and A. T. Young (1972), The Viking missions to Mars, *Icarus*, *16*, 1–16, doi:10.1016/0019-1035(72)90133-9.

Squyres, S. W., and A. H. Knoll (2005), Sedimentary rocks at Meridiani Planum: Origin, diagenesis, and implications for life on Mars, *Earth Planet. Sci. Lett.*, *240*, 1–10, doi:10.1016/j.epsl.2005.09.038.
Squyres, S. W., et al. (2004), In situ evidence for an ancient aqueous environment at Meridiani Planum, Mars, *Science*, *306*, 1709–1714, doi:10.1126/science.1104559.
Squyres, S. W., et al. (2007), Pyroclastic activity at home plate in Gusev Crater, Mars, *Science*, *316*, 738–742, doi:10.1126/science.1139045.
Squyres, S. W., et al. (2009), Exploration of Victoria Crater by the Mars Rover Opportunity, *Science*, *324*, 1058–1061, doi:10.1126/science.1139045.
Trebi-Ollennu, A., A. L. Rankin, Y. Cheng, K. S. Tso, R. G. Deen, H. Aghazarian, E. A. Kulczycki, R. G. Bonitz, and L. Alkalai (2013), Instrument deployment testbed: For planetary surface geophysical exploration, In Aerospace Conference, 2013 IEEE (pp. 1–14). IEEE.
Uwaerts, D. (2006), STAR 1000 detailed specification. Fill factory image sensors, Document number: APS-FF-DU-03-004, Issue 2. Available from the ESA European Space Components Information Exchange System. [Available at www.escies.org/.]
Van Gorp, B., P. Mouroulis, D. Blaney, R. O. Green, B. L. Ehlmann, and J. I. Rodriguez (2014), Ultra-compact Imaging Spectrometer for remote, in-situ, and microscopic planetary mineralogy, *J. Appl. Remote Sens.*, *8*, 1, 084988, doi:10.1117/1.JRS.8.084988.
Vaniman, D. T., et al. (2014), Mineralogy of a mudstone at Yellowknife Bay, Gale Crater, Mars, *Science*, *343*, 6169, doi:10.1126/science.1243480.
Viking Lander Team (1978), *The Martian Landscape*, NASA Spec. Publ., SP-425, 160 pp.
Wall, S. D., E. E. Burcher, and D. J. Jobson (1975), Reflectance characteristics of the Viking Lander camera reference test charts, in NASA Tech. Memo. 1975, NASA, Langley Res. Centre.
Weitz, C. M., et al. (2010), Visible and near-infrared multispectral analysis of geochemically measured rock fragments at the Opportunity landing site in Meridiani Planum, *J. Geophys. Res.*, *115*, E00F10, doi:10.1029/2010JE003660.